Determining the Jahn-Teller stabilization energy of adatom vacancies on a Si(111)-$\sqrt{3} \times \sqrt{3}$:B surface

Daejin Eom,[*] Chang-Youn Moon, and Ja-Yong Koo[†]
Korea Research Institute of Standards and Science, Yuseong, Daejeon 34113, Republic of Korea

(Received 24 April 2019; revised manuscript received 5 July 2019; published 3 September 2019)

A charged vacancy on the Si surface, which generates deep levels within the band gap to accommodate multiple charge states, becomes increasingly important with the device scaling. Yet its characteristics have not been addressed as comprehensively as the bulk vacancy in Si. Here we generate the adatom vacancies on a heavily B doped Si(111) surface and measure their structural and electronic properties by using scanning tunneling microscopy. We find that they are Jahn-Teller distorted in the ground state but undergo the symmetry-restoring transition when gated by the external bias. We also determine the stabilization energy of the Jahn-Teller transition as well as the hopping energy between the dangling bonds of the adatom vacancy quantitatively.

DOI: 10.1103/PhysRevB.100.115302

I. INTRODUCTION

The charged defects on the silicon surface become increasingly important with the device scaling in the nanometer ranges in which many efforts are carried out to exploit the surface channel instead of the buried one to cope with the short-channel effects [1,2]. Among such defects is the so-called adatom vacancy (AV), which is produced rather easily by energetic particles or electric fields owing to the weak bonding of the adatoms compared to other surface atoms [3–5]. This AV often exhibits different characteristics from the bulk vacancy in Si because its behavior is significantly influenced by the Fermi level E_F pinning on the surface or by the surface-state evolution within the band gap [6]. For example, the bulk vacancy in Si shows the Jahn-Teller (JT) distortion depending on the bulk E_F [7,8], whereas the AV on the Si(111)-7 × 7 surface (or, simply, 7 × 7 surface) has not displayed any evidence of the symmetry-lowering distortion so far [5,6,9].

The (111) surfaces of Si, on the other hand, have the $\sqrt{3} \times \sqrt{3}$ structure instead of the 7 × 7 one when they are heavily doped with boron [10–12]. This Si(111)-$\sqrt{3} \times \sqrt{3}$ surface (or, simply, $\sqrt{3} \times \sqrt{3}$ surface) does not evolve an energy state within the band gap, in contrast to the 7 × 7 surface [12]. Also, E_F is positioned near the valence band maximum on the $\sqrt{3} \times \sqrt{3}$ surface, whereas it is pinned in the middle of the gap on the 7 × 7 one [12]. Hence, the AVs on the two surfaces may have dissimilar characteristics. Yet their details, including the bias-driven Jahn-Teller transition, if any, and the relevant energy gain, have not been uncovered until now. In fact, it would be a challenging task to address such characteristics comprehensively because the AVs on the two surfaces evolve deep levels within the band gap, as does the bulk vacancy, and accommodate multiple charge states via the substantial rearrangement of atomic positions and electron densities [7,8,13–15].

Here we employ the atom manipulation technique to generate the AVs on the $\sqrt{3} \times \sqrt{3}$ surface and investigate their structural and electronic properties by using scanning tunneling microscopy and spectroscopy (STM/S). We find that, unlike the 7 × 7 surface, the AVs on the $\sqrt{3} \times \sqrt{3}$ surface are JT distorted in the ground state but undergo the symmetry-restoring transition when gated by the external bias. We also determine the energy gain or stabilization energy of the JT transition as well as the hopping energy between the dangling bond (DB) orbitals of the AVs quantitatively. These findings will extend our knowledge on the surface vacancies on Si beyond the 7 × 7 surface and will eventually contribute to fabricating better-performing nanometer-scale devices.

II. EXPERIMENT

Our experiments were carried out using low-temperature STM in an ultrahigh-vacuum chamber, whose base pressure was below 1×10^{-10} Torr. Heavily B doped crystalline Si with the (111) orientation and a resistivity of <0.01 Ω cm was cleaned *in situ* by repeated thermal flashes at ∼1200 °C. It was then cooled down to the room temperature at a rate of ∼2 K/s after the last flash. After that, it was quenched down to ∼4.5 K for the STM/S measurements. The STM probe tip was made of Pt-Ir alloy.

III. RESULTS

Shown in Fig. 1(a) is the STM topography of a Si(111) surface which has a $\sqrt{3} \times \sqrt{3}$ reconstruction because of the heavy B population in the surface region [10–12]. Its structural model is illustrated in Fig. 1(c), where the topmost Si adatom sits at the fourfold-coordinated top site (T_4 site) and a B atom occupies the fivefold-coordinated substitutional site (S_5 site) directly below the Si adatom [10,11]. Figure 1(a) also contains a natural defect (Si_B), as indicated by the arrow, for which a Si atom substitutes the B atom at the S_5 site to produce

[*]d.eom@kriss.re.kr
[†]koojayon@kriss.re.kr

 ©2019 American Physical Society

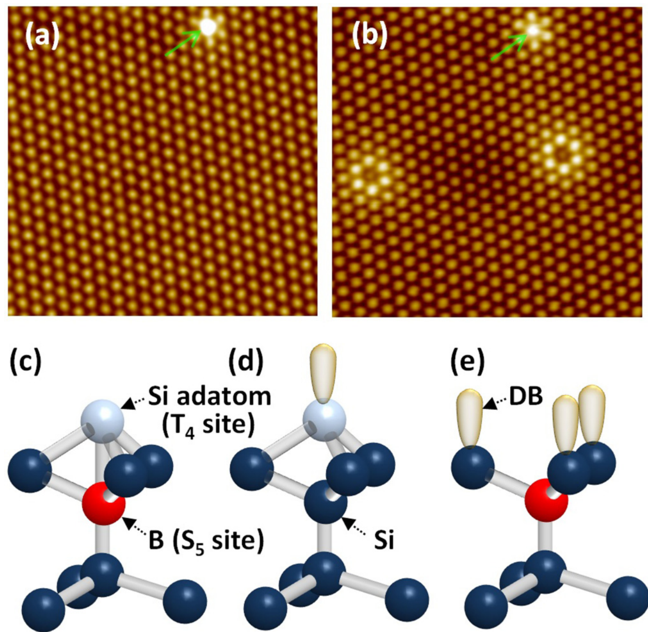

FIG. 1. (a) Topography of a heavily B doped Si(111)-$\sqrt{3} \times \sqrt{3}$ surface, whose lateral dimension is 15 × 15 nm^2. It is probed with a sample bias V_{sample} of 3.0 V and a tunneling current I_t of 0.1 nA. The bright feature indicated by the arrow is a point defect (Si_B defect) that is produced during the sample annealing process. (b) Topography of the same area as that in (a), but taken after two Si adatoms are removed by the application of V_{pulse}. It is probed with $V_{\text{sample}} = 2.8$ V and $I_t = 0.1$ nA. Structural models of (c) a Si adatom, (d) a Si_B defect, and (e) the AV, respectively. The blue (red) ball is a Si (B) atom. The pale blue ball represents a Si adatom. The prolate ellipsoid is the Si DB.

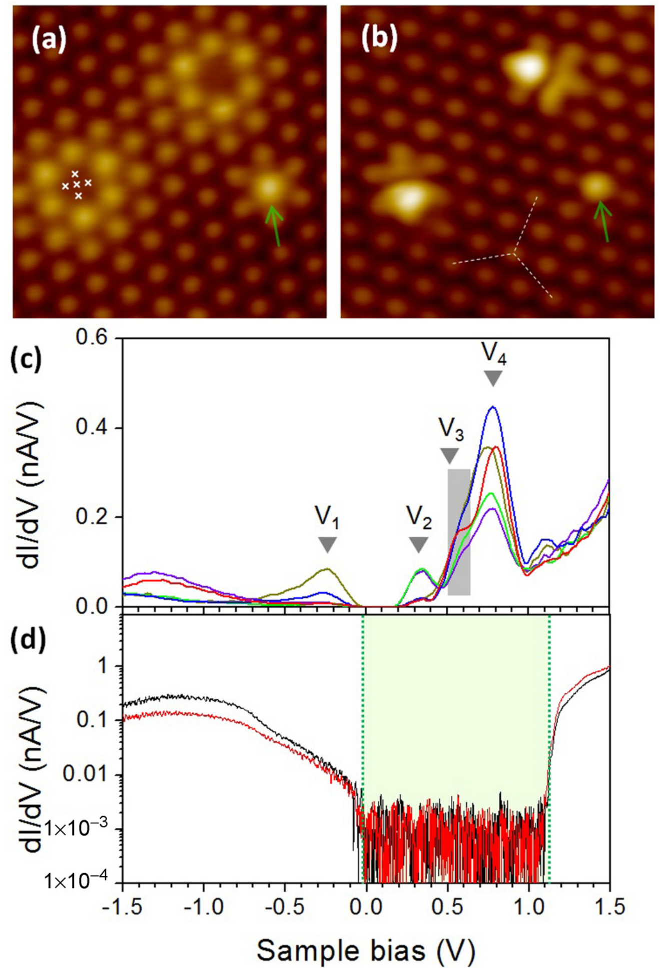

FIG. 2. (a) and (b) Both images are taken in the same area, whose lateral dimension is 6.5 × 6.5 nm^2. The image in (a) [(b)] is probed with $V_{\text{sample}} = 2.5$ V (−1.0 V) and $I_t = 0.6$ nA. The Si_B defect is indicated by the arrow and is used as a reference. The dashed lines in (b) denote the $\langle 1\bar{1}0 \rangle$ directions. (c) dI/dV spectra probed at five different positions within the AV as marked by the crosses in (a). They are displayed in linear scale along the vertical axis. The triangles indicate four distinct spectral features at the sample biases of $V_1 = -0.23$ V, $V_2 = 0.34$ V, $V_3 = 0.51$ V, and $V_4 = 0.79$ V. (d) dI/dV spectra probed on the normal $\sqrt{3} \times \sqrt{3}$ surface, i.e., on top of Si adatoms (red line) and in the threefold hollow sites (black line). They are displayed in logarithmic scale along the vertical axis. The dotted lines at $V_{\text{sample}} = -0.02$ and 1.12 V indicate the band edges.

a DB orbital at the T_4 site [see Fig. 1(d)]. We then generate the AVs on the $\sqrt{3} \times \sqrt{3}$ surface intentionally by employing an atom manipulation technique similar to that of Lyo and Avouris [3]: The STM tip is placed above a specific Si adatom, and a high-field bias pulse V_{pulse} is applied on it with the feedback loop off [16], which causes the adatom under the STM tip to be kicked out to produce the vacancy structure at the T_4 site. The STM topography of such produced AVs is displayed in Fig. 1(b), and its structural model is shown in Fig. 1(e), where newly exposed Si atoms in the second layer generate three DB orbitals with the 1 × 1 spacing of the (111) surface.

The STM topographies in Figs. 2(a) and 2(b) contain two AVs and one Si_B defect, which are taken over the same region but give polarities opposite the sample bias. The AVs in the empty-state topography [see Fig. 2(a)] are featureless and compatible with the threefold symmetry or C_{3v} point group symmetry of the $\sqrt{3} \times \sqrt{3}$ surface. On the other hand, the same AVs exhibit internal features in the filled-state topography [see Fig. 2(b)], which have mirror symmetry or C_s point group symmetry with the mirror plane perpendicular to the $\langle 1\bar{1}0 \rangle$ direction. This symmetry reduction from C_{3v} to C_s implies that the AV undergoes a substantial relaxation when the sample bias changes from the empty-state condition (i.e., 2.5 V) to the filled-state one (i.e., −1.0 V), as is discussed in detail later. We also measure the energy levels of the AV by using the STS technique. Shown in Fig. 2(c) is the differential conductance (dI/dV) spectra measured at five different positions within the AV, which exhibits several spectroscopic features, as indicated by the triangular symbols: A strong peak at V_4 and three relatively weak features at V_1, V_2, and V_3. These spectra are in contrast to the dI/dV spectrum measured on the normal $\sqrt{3} \times \sqrt{3}$ surface [see Fig. 2(d)], which does not evolve an energy state within the Si band gap.

The spatial symmetry of each energy state in Fig. 2(c) is unraveled by visualizing its squared wave function, that is, by measuring the dI/dV map around the AV at the corresponding sample bias. The results are displayed in Figs. 3(b)–3(e) together with the simultaneously probed topography in

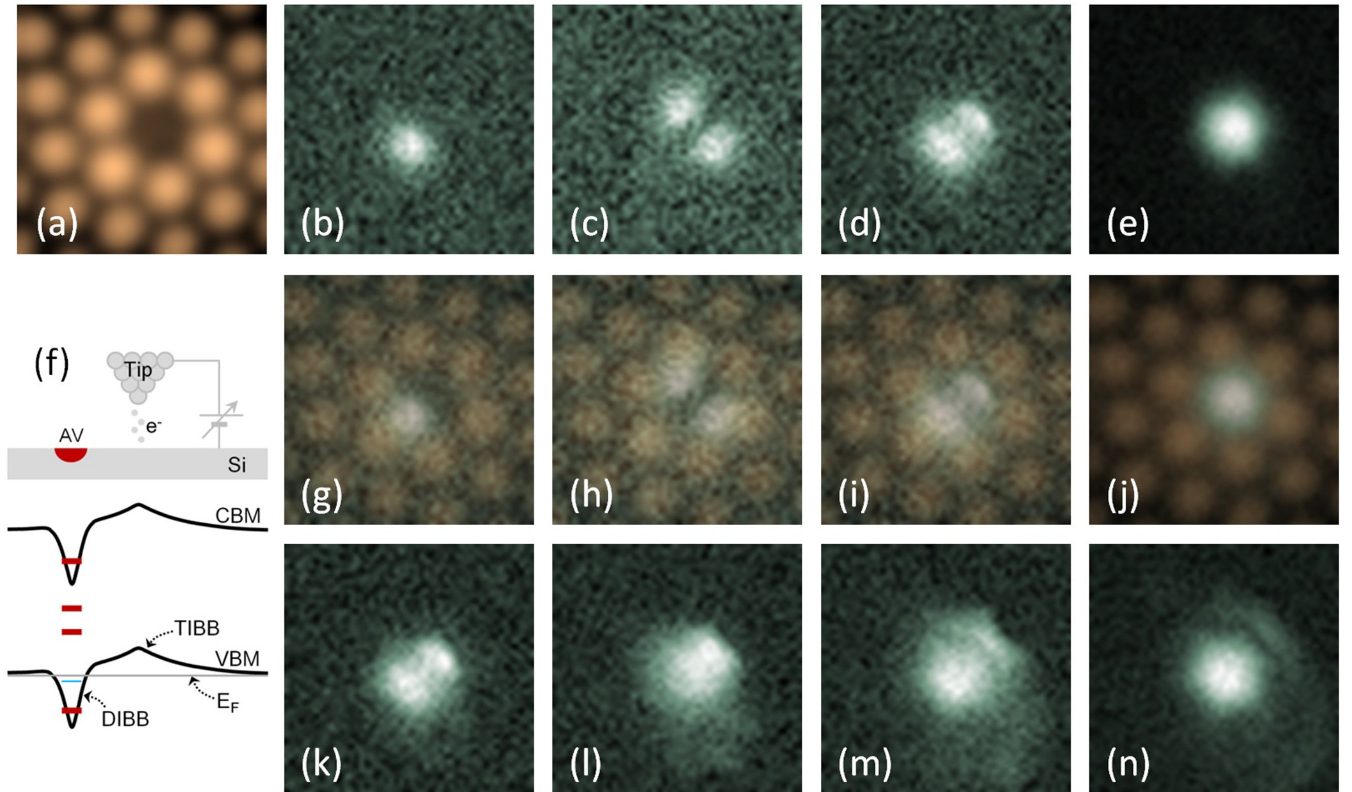

FIG. 3. (a) Topography of an AV on the $\sqrt{3}\times\sqrt{3}$ surface, whose lateral dimension is 3×3 nm^2. It is imaged with $V_{\text{sample}} = 2.5$ V and $I_t = 1.0$ nA. (b)–(e) Four dI/dV maps measured in the same area as that in (a). The sample bias during the dI/dV measurement is (b) $V_1 = -0.23$ V, (c) $V_2 = 0.34$ V, (d) $V_3 = 0.51$ V, and (e) $V_4 = 0.79$ V. (f) Schematic of the TIBB, which is centered at the tip position and is superimposed by the DIBB. The red (blue) segment is the energy (charge transition) level of the AV. (g)–(j) The same images as those in (b)–(e), respectively, but overlaid with the topography in (a). (k)–(n) dI/dV maps measured in the same area as that in (a). The sample bias during the dI/dV measurements is (k) 0.52 V, (l) 0.56 V, (m) 0.61V, and (n) 0.66 V.

Fig. 3(a). Figures 3(g)–3(j) are the same images as those in Figs. 3(b)–3(e), respectively, but are overlaid by the topography in Fig. 3(a). The squared wave function of the uppermost gap state at V_4 [see Fig. 3(e)] has a radial density distribution about the center of the AV and is compatible with the threefold symmetry of the $\sqrt{3}\times\sqrt{3}$ surface, as is the empty-state topography in Fig. 2(a). On the other hand, the squared wave functions of the resonance state at V_1 [see Fig. 3(b)] and the low-lying gap states at V_2 and V_3 [see Figs. 3(c) and 3(d)] have reduced C_s symmetry, as does the filled-state topography in Fig. 2(b). Hence, the energy states in Fig. 2(c) also exhibit the symmetry change from C_{3v} to C_s like the topography. We ascribe this symmetry change to the JT transition driven by the charge-state change of the AV; that is, the AV is JT distorted in the ground state with a specific charge state which is maintained up to $V_{\text{sample}} \leqslant 0.51$ V but restores the C_{3v} symmetry at the enhanced sample biases (i.e., $V_{\text{sample}} > 0.51$ V) by changing its charge state to another value via the tip-induced band bending (TIBB). In fact, the dI/dV maps taken in the gray rectangular region in Fig. 2(c) (i.e., $V_{\text{sample}} = 0.52$–0.66 V) evolve a faint feature around the AV, as displayed in Figs. 3(k)–3(n), whose size grows with the sample bias. It is indicative of the discharging process via the TIBB during the STS measurements [16–18]: A large enough positive sample bias causes the band to bend upward near the AV, as illustrated in Fig. 3(f), and, eventually, makes an occupied defect state of the AV lose an electron to the bulk states by causing its charge transition level to cross E_F. It then alters the electrostatic potential around the AV to result in a current jump or, equivalently, the conductance enhancement. Since the band bending at the AV position is less effective when the tip position is farther from it, such a discharging process would occur with a larger sample bias at a farther tip position from the AV, which is consistent with the behavior in Figs. 3(k)–3(n). It is noteworthy that the TIBB is superimposed by the defect-induced band bending (DIBB) in Fig. 3(f) because a previous study [16] revealed that the AV is positively charged, not neutral, in the ground state; that is, three DBs of the AV have either one or zero electron in them, with the underlying B atom being singly negatively charged.

To elaborate on the above mechanism further, we illustrate, in Fig. 4(a), the energy levels of three DB orbitals of the AV under the relevant symmetries. Centered at $Q = Q_{3v}$ are the energy levels of three DB orbitals in the C_{3v} symmetry for which the effective hopping integral t_{eff} between two DB orbitals is assumed to be negative because of the indirect nature of the electron hopping between them (see Appendix A for further discussion). This makes the doubly degenerate (E_e) level have a lower energy than nondegenerate (E_a) level,

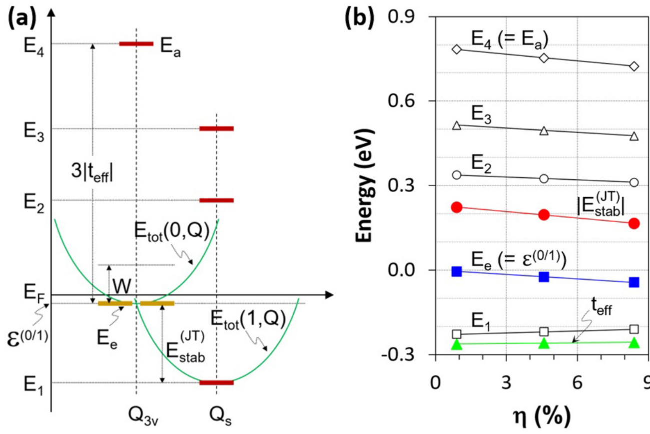

FIG. 4. (a) Schematic of the AV's energy levels. The vertical axis is the energy relative to E_F. The horizontal axis is the configuration coordinates Q, with Q_{3v} (Q_s) representing the AV structure with the C_{3v} (C_s) symmetry. At $Q = Q_{3v}$, the AV's three DB orbitals evolve a doubly degenerate E_e level and nondegenerate E_a level with an energy separation of $3|t_{eff}|$. The effective hopping integral t_{eff} is assumed to be negative. W is the Coulomb repulsion energy when two electrons occupy two different E_e states. At $Q = Q_s$, the E_e level with one electron lifts its degeneracy to gain the JT stabilization energy $E_{stab}^{(JT)}$ and to evolve three distinct levels, E_1, E_2, and E_3. $\epsilon^{(0/1)}$ is the transition level where the number of electrons in three DB orbitals changes from 0 to 1. $E_{tot}(n, Q)$ is the total formation energy of the AV when it is in the Q configuration and has n (=0 or 1) electrons in three DB orbitals. The energy levels in red (orange) are directly accessible (inaccessible) in the STM/S measurements. (b) Variations of the energy parameters in (a) as a function of TIBB η. The quantities with solid symbols are not directly observable by the STM/S measurements.

as illustrated in Fig. 4(a). The associated eigenfunctions are written as

$$\Psi_a = (\phi_1 + \phi_2 + \phi_3)/\sqrt{3 + 6S}, \qquad (1)$$

$$\Psi_{e2} = (\phi_2 - \phi_3)/\sqrt{2 - 2S}, \qquad (2)$$

$$\Psi_{e1} = (2\phi_1 - \phi_2 - \phi_3)/\sqrt{6 - 6S}, \qquad (3)$$

where ϕ_i is the ith DB orbital and S is the overlap integral between them. As mentioned above, these DB orbitals have, at most, one electron in them in total because the AV is positively charged in the ground state [16]. If the E_e level goes below E_F to accommodate one electron but not two due to the Coulomb repulsion energy W [19], then it will induce the JT transition to lift the orbital degeneracy. When this transition takes place in a way compatible to the C_s symmetry [see the $Q = Q_s$ line in Fig. 4(a)], the eigenfunctions in Eqs. (1)–(3) would be modified as

$$\Psi_3 = [\alpha\phi_1 + (\phi_2 + \phi_3)]/\sqrt{2 + 2S + 4S\alpha}, \qquad (4)$$

$$\Psi_2 = (\phi_2 - \phi_3)/\sqrt{2 - 2S}, \qquad (5)$$

$$\Psi_1 = [2\phi_1 - \beta(\phi_2 + \phi_3)]/\sqrt{4 - 8S\beta}, \qquad (6)$$

where $|\alpha|, |\beta| \ll 1$. The eigenfunctions in Eqs. (5) and (6), when squared [see Figs. 6(e) and 6(d) in Appendix B], resemble the dI/dV maps in Figs. 3(c) and 3(b), respectively, suggesting that the AV is JT distorted in the C_s-symmetric fashion in the ground state by holding one electron in the E_e level [20]. On the other hand, if the TIBB is strong enough near the AV, its charge transition level $\epsilon^{(0/1)}$ [see Fig. 4(a)], where the number of electrons in three DB orbitals changes from 0 to 1, will align with E_F at a specific sample bias and, as a consequence, contribute an additional channel for the charge flow from the tip to the sample. Indeed, the dI/dV map at V_3 [see Fig. 3(d)] is not simply $|\Psi_3|^2$ but is superimposed by $|\Psi_1|^2$. This implies that $\epsilon^{(0/1)}$ is quite close to E_F at this sample bias, so that Ψ_1 as well as Ψ_3 contributes to the tunneling process significantly: In the early stage of the discharging process, the electron in Ψ_1 starts to gain some probability to escape to the bulk E_F even though it still has a larger probability to stay in Ψ_1 so that, on average, the AV maintains the JT-distorted structure. This dynamic condition, i.e., electron escape from Ψ_1 followed by the electron refilling into it, will make the Ψ_1 state an effective path for the charge flow between the tip and the sample. At the same time, the tip's chemical potential aligns with the energy level of Ψ_3 by accident, providing another channel for the electron flow from the tip to the sample. Hence, both Ψ_1 and Ψ_3 states would work as the effective tunneling paths in the early stage of the discharging process. Once the electron in the Ψ_1 state escapes to the substrate after a further increase of the sample bias [see Figs. 3(k)–3(n)], the AV will lose the energy gain for the JT distortion and restore the C_{3v} symmetry of the $\sqrt{3} \times \sqrt{3}$ surface. Hence, the spectroscopic features above the gray rectangular region in Fig. 2(c) would have C_{3v} symmetry, as does the uppermost gap state at V_4 [see Fig. 3(e)]. Indeed, this state corresponds to the E_a level in Fig. 4(a).

Now we determine the energy parameters in Fig. 4(a) quantitatively. First, the amount of band bending η caused by a sample bias of 1 V is deduced by comparing the Si band gap measured via the STS technique $E_g^{(STS)}$ with the value that does not suffer from the band-bending effect. The former is 1.14 ± 0.02 eV at 4.5 K, as determined from Fig. 2(d) (see Appendix C for more detail). The latter is given by, e.g., the optical measurements, whose result ($E_g^{(optical)}$) is 1.09 ± 0.02 eV for heavily [i.e., $(1\text{–}2) \times 10^{19}$ cm^{-3}] B doped Si substrates when measured at low temperatures (<20 K) (see Appendix C for more details). The two gap values yield the η value, that is, $\eta = E_g^{(STS)}/E_g^{(optical)} - 1 = 0.046 \pm 0.037$. This value indicates that the TIBB is rather weak (<9%) on the $\sqrt{3} \times \sqrt{3}$ surface, as expected from the heavily doped nature. Nevertheless, this weak effect needs to be subtracted from the sample biases when we determine the intrinsic energy levels like those in Fig. 4(a): $E_i = (1 - \eta) \times eV_i$ ($i = 1, 2, 3, 4$). Such derived E_1, E_2, E_3, and E_4 (= E_a) levels are displayed in Fig. 4(b) as functions of η around its median value (0.046). The charge transition level $\epsilon^{(0/1)}$ of the AV also shifts to E_F at $V_{sample} \simeq 0.52$ V by the TIBB [see Figs. 3(k)–3(n)]. Thus, we get $\epsilon^{(0/1)} = -\eta \times eV_{sample} \simeq -0.024 \pm 0.020$ eV [see Fig. 4(b)], which is slightly below E_F. On the other hand,

$\epsilon^{(0/1)}$ is decomposed as

$$\epsilon^{(0/1)} = E_{\rm tot}(1, Q_s) - E_{\rm tot}(0, Q_{3v}) = [E_{\rm tot}(1, Q_s) - E_{\rm tot}(0, Q_s)] + [E_{\rm tot}(0, Q_s) - E_{\rm tot}(0, Q_{3v})]. \quad (7)$$

Here $E_{\rm tot}(n, Q)$ is the total formation energy of the AV when it is in the Q configuration and has n electrons in three DB orbitals. The first square brackets in Eq. (7) are the filled-state energy level in the $Q_{\rm s}$ configuration and therefore are identical to the E_1 level in Fig. 4(a). The second ones are the elastic energy cost $E_{\rm elas}^{\rm (JT)}$ due to the configuration change from $Q_{\rm 3v}$ to $Q_{\rm s}$. These E_1 and $E_{\rm elas}^{\rm (JT)}$ values can be determined explicitly by utilizing the functional form of $E_{\rm tot}(n, Q)$ and realizing that the free electron of the ionized state resides at the Fermi level:

$$E_{\rm tot}(0, Q) = E_F + \tfrac{1}{2}k(Q - Q_{3v})^2 = \tfrac{1}{2}k(Q - Q_{3v})^2, \quad (8)$$

$$E_{\rm tot}(1, Q) = E_e - g(Q - Q_{3v}) + \tfrac{1}{2}k(Q - Q_{3v})^2 = E_e - \tfrac{1}{2}g^2/k + \tfrac{1}{2}k(Q - Q_{3v} - g/k)^2, \quad (9)$$

where k (g) is the spring constant (the electron-lattice coupling parameter) and $E_{\rm F}$ is set to zero. Then the E_1 level in Fig. 4(a) is obtained by minimizing Eq. (9), i.e., by setting $Q = Q_{\rm 3v} + g/k$ $(=Q_{\rm s})$ in Eq. (9), which gives $E_1 = E_{\rm e} - g^2/2k$. Also, the elastic energy cost $E_{\rm elas}^{\rm (JT)}$ is obtained by setting $Q = Q_{\rm s}$ in Eq. (8). It gives $E_{\rm elas}^{\rm (JT)} = +g^2/2k = E_{\rm e} - E_1$. Therefore, the right-hand side in Eq. (7) becomes $E_1 + E_{\rm elas}^{\rm (JT)} = E_1 + (E_{\rm e} - E_1) = E_{\rm e}$, meaning that $\epsilon^{(0/1)}$ is positioned at the $E_{\rm e}$ level, as illustrated in Fig. 4(a). Thus, $E_{\rm e} = \epsilon^{(0/1)} \simeq -0.024 \pm 0.020$ eV. This, in turn, enables us to determine the JT stabilization energy $E_{\rm stab}^{\rm (JT)}$ in Fig. 4(a): $E_{\rm stab}^{\rm (JT)} = E_1 - E_{\rm e} \simeq -0.20 \pm 0.03$ eV. The theoretical calculations [8] reveal that the bulk vacancy in Si with one electron occupying the triply degenerate level has a JT stabilization energy of 0.17–0.21 eV. These values are comparable to the $E_{\rm stab}^{\rm (JT)}$ value of the AV, although the latter differs from the bulk vacancy in several aspects, including the geometry, the number of DBs, and the chemical species near the vacancy. Also, the effective hopping integral $t_{\rm eff}$ between two DB orbitals of the AV can be deduced from the above parameters: $t_{\rm eff} = (1/3)(E_{\rm e} - E_{\rm a}) \simeq -0.26 \pm 0.01$ eV (see Appendix A for more details). This is smaller in magnitude and opposite in polarity than that of the bulk vacancy in Si ($t^{\rm (bulk)} = +0.45$ eV from the A_1-T_2 splitting [21,22]). The reason is partly because the DB orbitals are oriented differently in the two cases; that is, they are parallel in the AV but head toward each other with an angle of 109.5° in the bulk vacancy. Thus, the overlap between two DB orbitals is rather weak (strong) in the former (latter). The reason is also partly because the acceptor state of the B atom at the S_5 site can mediate the electron hopping between two DB orbitals in the former case (see Appendix A). Hence, the indirect hopping via the B atom (direct hopping between two DB orbitals) becomes more efficient for the former (latter; see Appendix A for further discussion).

IV. CONCLUSION

We have generated the AVs on the $\sqrt{3} \times \sqrt{3}$ surface and measured its dI/dV spectra and maps using the STM/S technique. They reveal that the AV is JT distorted to have a reduced $C_{\rm s}$ symmetry in the ground state but undergoes a symmetry ($C_{\rm 3v}$) restoring transition at $V_{\rm sample} \simeq 0.52$ V by the TIBB. The energy gain or stabilization energy $E_{\rm stab}^{\rm (JT)}$ due to the JT transition is experimentally determined to have a value of -0.20 ± 0.03 eV. This is comparable to the theoretical estimate for the JT stabilization energy of the bulk vacancy in Si. These findings will extend our knowledge of the surface vacancies on Si and, possibly, will contribute to fabricating better-performing nanometer-scale devices.

ACKNOWLEDGMENTS

This work was supported by the basic R&D program of the Korea Research Institute of Standards and Science, and partly by the Basic Science Research Program of the National Research Foundation of Korea (NRF) funded by the Ministry of Science and ICT (2016R1C1B1014715).

APPENDIX A: EFFECTIVE HOPPING INTEGRAL BETWEEN DB ORBITALS

The electron hopping between two DB orbitals can take place either in a direct way or via the substrate states (i.e., in an indirect way). The former is responsible for many chemical bonds where the bonding (symmetric) state has a lower energy than the antibonding (antisymmetric) one and decays exponentially with the distance between two orbitals. On the other hand, the latter is caused by the coupling of the two DB orbitals to the substrate's electronic states and possibly leads to the long-range interaction with much slower (power-law) decay than the former one [23].

In the main text, we assumed that the electron hopping between two DB orbitals of the AV has an indirect nature; that is, the indirect hopping via the substrate states is more effective than the direct transfer between them. To grasp this point in a more concrete way, we calculate the energy levels of the model structure in Fig. 5, where the Si-B distance is shorter than the Si-Si separation. Then, its Hamiltonian is written as

$$H = \varepsilon_d \sum_i c_i^\dagger c_i + \varepsilon_s c_s^\dagger c_s - t_d \sum_{<ij>} (c_i^\dagger c_j + {\rm H.c.}) - t_s \sum_i (c_i^\dagger c_s + {\rm H.c.}), \quad ({\rm A1})$$

where ε_d and ε_s are the energies of the DB orbitals ($\phi_{\rm i}$, $i = 1, 2, 3$) and substrate state $\varphi_{\rm s}$, respectively, and c_i $(i = 1, 2, 3)$ and c_s annihilate an electron in $\phi_{\rm i}$ and $\varphi_{\rm s}$, respectively. Also, t_d (t_s) is the "direct" hopping integral between $\phi_{\rm i}$ and $\phi_{\rm j}$ ($\varphi_{\rm s}$). Here we assume that $t_s > t_d > 0$; that is, the hopping interaction between DB and substrate states is stronger than that between two DB orbitals. Also, we assume that $\varepsilon_d > \varepsilon_s$ since we are dealing with the case where the DB (substrate) state is within the band gap (valence band). The Hamiltonian

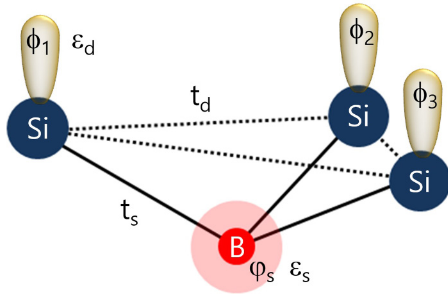

FIG. 5. Structural model for the electron hopping. The Si atom sits in three vertices of an equilateral triangle (dotted line), and the substrate atom (indicated by a B) is located below the triangle such that the distances from all Si atoms (solid line) are identical. ϕ_i ($i = 1, 2, 3$) is the DB orbital on the ith Si atom, and φ_s represents the substrate state centered on the B atom. ε_d (ε_s) is the energy level of ϕ_i (φ_s). t_d is the hopping integral between ϕ_i and ϕ_j ($i \neq j$), and t_s is between ϕ_i and φ_s.

in Eq. (A1) is solved to give the doubly degenerate E_0 level and nondegenerate E_+ and E_- levels:

$$E_0 = \varepsilon_d + t_d, \tag{A2}$$

$$E_\pm = \tfrac{1}{2}\left[(\varepsilon_d + \varepsilon_s - 2t_d) \pm \sqrt{(\varepsilon_d - \varepsilon_s - 2t_d)^2 + 12t_s^2}\right]. \tag{A3}$$

The corresponding eigenfunctions, $\Psi_0^{(1)}$, $\Psi_0^{(2)}$ (for the E_0 level), Ψ_+ (for the E_+ level), and Ψ_- (for the E_- level), are written as

$$\Psi_0^{(1)} = (2\phi_1 - \phi_2 - \phi_3)/\sqrt{6 - 6S},$$
$$\Psi_0^{(2)} = (\phi_2 - \phi_3)/\sqrt{2 - 2S}, \tag{A4}$$

$$\Psi_\pm = [(\phi_1 + \phi_2 + \phi_3) + p_\pm \varphi_s]/\sqrt{N_\pm}, \tag{A5}$$

with

$$p_\pm = \frac{1}{2t_s}\left[(\varepsilon_d - \varepsilon_s - 2t_d) \mp \sqrt{(\varepsilon_d - \varepsilon_s - 2t_d)^2 + 12t_s^2}\right], \tag{A6}$$

where $N_\pm$ are the normalization constants.

The eigenfunctions in Eqs. (A4) and (A5) indicate that the energy levels, E_-, E_+, and E_0, have the bonding, antibonding, and nonbonding characters, respectively, between the substrate state φ_s and three DB orbitals ϕ_i. Since we are dealing with the case where φ_s (ϕ_i) is initially occupied (unoccupied), the lowest E_- level should be filled by the electrons, whereas the E_0 and E_+ levels should be empty. Now we restrict our attention to the empty states, that is, $\Psi_0^{(1)}$, $\Psi_0^{(2)}$, and Ψ_+. If we take into account only the DB (ϕ_i) components of $\Psi_0^{(1)}$, $\Psi_0^{(2)}$, and Ψ_+, then such projected states onto the DB orbitals become the eigenfunctions of the following effective Hamiltonian:

$$H_{\text{eff}} = \varepsilon_d \sum_i c_i^\dagger c_i - t_{\text{eff}} \sum_{\langle ij \rangle} (c_i^\dagger c_j + \text{H.c.}), \tag{A7}$$

where t_{eff} is an effective hopping integral such that $3t_{\text{eff}} = E_0 - E_+$. It is noteworthy that the effective hopping integral t_{eff} in Eq. (A7) is not identical to the real (direct) hopping integral t_d in Eq. (A1) but is introduced to fit the energy difference between doubly and nondegenerate empty levels in Eqs. (A2) and (A3). Thus, unlike t_d in Eq. (A1), t_{eff} in Eq. (A7) can have a negative value if $E_0 < E_+$. From Eqs. (A2) and (A3),

$$E_0 < E_+ \quad \text{if} \quad \varepsilon_d - \varepsilon_s < \left(t_s^2 - t_d^2\right)/t_d. \tag{A8}$$

This implies that the effective hopping integral t_{eff} in Eq. (A7) would be negative if the direct hopping integral t_s between DB and substrate states is much stronger than the direct hopping integral t_d between two DB orbitals.

As for the AV structure in the main text, the distance (3.84 Å) between two DB orbitals is 1.63 times larger than the nearest-neighbor distance (2.35 Å) of Si (i.e., the Si-B separation in Fig. 5). According to the theoretical calculations [24,25], ($pp\pi$) and ($ss\sigma$), which are the most relevant Slater-Koster parameters of Si for the parallel geometry like the DB orbitals of the AV, become ~7 times smaller when the separation between two Si atoms increases by the same amount, i.e., from 2.35 to 3.84 Å. Such a strong dependence of Slater-Koster parameters on the separation would make multiple or repeated hoppings over the nearest-neighbor distance (2.35 Å) more effective than the direct hopping over larger distance (3.84 Å). In addition, the acceptor state (not the $2sp^3$ orbital) of the B atom can mediate the electron hopping between two DB orbitals. This acceptor state has a $1s$ orbital with an effective Bohr radius of ~13 Å [26], and thus, its overlap with a DB orbital would be quite large when compared to the direct overlap between two DB orbitals. Hence, the electron hopping via the acceptor state would be very significant, helping the indirect hopping via the B atom to exceed the direct hopping between two DB orbitals too. These two mechanisms would satisfy the criterion of Eq. (A8) for the AV structure. Thus, the AV will have a negative value for the effective hopping integral t_{eff} between two DB orbitals, as assumed in the main text.

APPENDIX B: WAVE FUNCTIONS OF THE EFFECTIVE HAMILTONIANS

If we set $t_{\text{eff}} = -0.26$ eV and $\varepsilon_d = +0.24$ eV in Eq. (A7), then the Hamiltonian has two eigenvalues, $E_e = -0.02$ eV (doubly degenerate) and $E_a = +0.76$ eV, and three eigenfunctions, Ψ_{e1}, Ψ_{e2}, and Ψ_a, whose squares are visualized in Figs. 6(a)–6(c).

The (squared) eigenfunctions in Fig. 6 are evaluated by assuming that each DB has the $3p_z$ orbital of Si instead of the $3sp^3$ hybrid for calculational simplicity. Indeed, the (squared) eigenfunctions of Eq. (A7) would yield spatial distributions similar to those in Figs. 6(a)–6(c) even though each DB has a $3s$ or $3sp^3$ [$= \frac{1}{2}(3s \text{ orbital}) + \frac{\sqrt{3}}{2}(3p \text{ orbital})$] orbital. Also the (squared) eigenfunctions in Fig. 6 are evaluated at a height of 5 Å above the reference plane which is defined by three Si nuclei.

Now we assume that the atomic structure in Fig. 5 undergoes the Jahn-Teller (JT) transition in a C_s-compatible way so that one of the three DBs has a dissimilar on-site energy and the other two have a different hopping integral. Then, Eq. (A7) is transformed to

$$H'_{\text{eff}} = \varepsilon_{d1} c_1^\dagger c_1 + \varepsilon_{d2}(c_2^\dagger c_2 + c_3^\dagger c_3) - t_{\text{eff}}(c_1^\dagger c_2 + c_1^\dagger c_3 + \text{H.c.}) - t'_{\text{eff}}(c_2^\dagger c_3 + \text{H.c.}). \tag{B1}$$

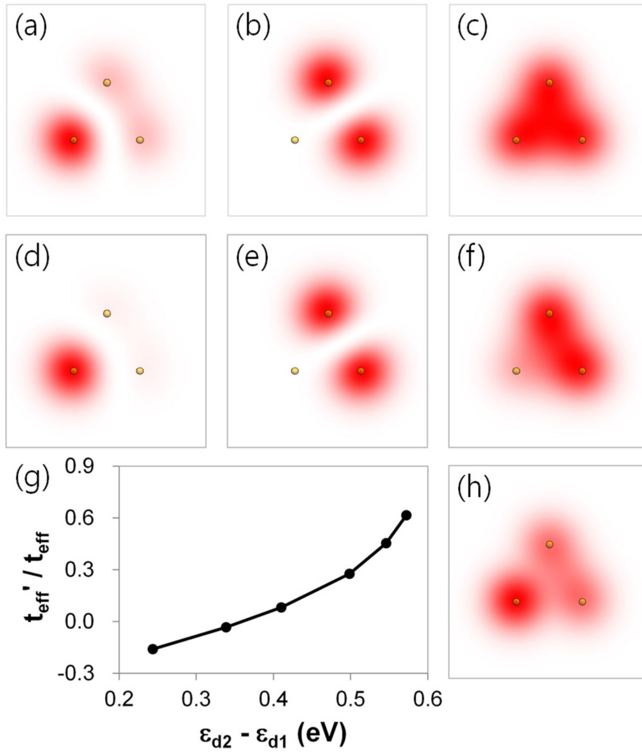

FIG. 6. (a)–(c) Squared eigenfunctions of Eq. (A7) with $\varepsilon_d = +0.24$ eV and $t_{\rm eff} = -0.26$ eV: (a) $|\Psi_{e1}|^2$, (b) $|\Psi_{e2}|^2$, and (c) $|\Psi_a|^2$. (d)–(f) Squared eigenfunctions of Eq. (B1) with $\varepsilon_{d1} = -0.13$ eV, $\varepsilon_{d2} = +0.37$ eV, $t_{\rm eff} = -0.17$ eV, and $t'_{\rm eff} = -0.05$ eV: (d) $|\Psi_1|^2$, (e) $|\Psi_2|^2$, and (f) $|\Psi_3|^2$. (g) A possible relation between various combinations of ε_{d1}, ε_{d2}, $t_{\rm eff}$, and $t'_{\rm eff}$ in Eq. (B1), which yield the same energy spectrum and similar eigenfunctions as those in (d)–(f). (h) Sum of (d) and (f), i.e., $|\Psi_1|^2 + |\Psi_3|^2$. The small circles in (a)–(f) and (h) represent the atomic positions of Si.

Here two different on-site energies, ε_{d1} and ε_{d2}, as well as two different hopping integrals, $t_{\rm eff}$ and $t'_{\rm eff}$, are introduced as the fitting parameters. If we set them as $\varepsilon_{d1} = -0.13$ eV, $\varepsilon_{d2} = +0.37$ eV, $t_{\rm eff} = -0.17$ eV, and $t'_{\rm eff} = -0.05$ eV, then the effective Hamiltonian in Eq. (B1) comes to have three different eigenvalues, i.e., $E_1 = -0.22$ eV, $E_2 = +0.32$ eV, and $E_3 = +0.50$ eV. These are indeed identical to the experimentally probed (and TIBB-compensated) energy values of the AV defect in the main text. The corresponding eigenfunctions, Ψ_1, Ψ_2, and Ψ_3, are visualized in Figs. 6(d)–6(f). Also we display $|\Psi_1|^2 + |\Psi_3|^2$ in Fig. 6(h) for comparison with Fig. 3(d) of the main text.

Generally, the JT transition is accompanied by the physical displacement of the constituent atoms from their original positions. However, we have assumed that the Si atoms are in their original (equilateral) positions when we evaluate the (squared) eigenfunctions in Figs. 6(d)–6(f) because, within our simple tight-binding model, it is not possible to determine the exact locations of the Si atoms after the JT transition. Nonetheless, the images in Figs. 6(d)–6(f) will still capture the essential features of the wave functions after the JT transition. On the other hand, the parameters ε_{d1}, ε_{d2}, $t_{\rm eff}$, and $t'_{\rm eff}$ in Eq. (B1) can have many different combinations to yield the same energy spectrum as the experimental ones in the main text (i.e., −0.22, 0.32, 0.50 eV), as illustrated in Fig. 6(g). In order to determine the right combination or to unravel more details of the JT transition, we need to adopt a more sophisticated calculation technique than our simple tight-binding model.

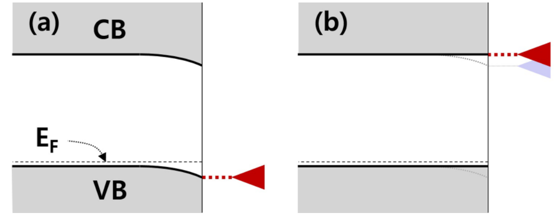

FIG. 7. (a) Example of the band profile when the bias (red triangle) is close to E_F. Here E_F is located near the VB edge. (b) Local band bending when the bias is raised up to the CB edge. The gray triangle indicates the position of the CB edge without the TIBB effect.

APPENDIX C: OPTICAL AND STS MEASUREMENTS OF THE Si BAND GAP

Generally, the band gap E_g of Si substrates varies with the doping concentration [27,28] and measurement temperature [29], that is,

$$E_g = E_g(0) - \Delta E_g(T) - \Delta E_g(n). \tag{C1}$$

Here $E_g(0)$ is the band gap of undoped (or lightly doped) Si substrates at zero (or sufficiently low) temperature, which is known to be 1.169 eV [30]. The second term in Eq. (C1) is the band gap narrowing due to the nonzero temperature and has the empirical formula $C \times T^2/(T + T_0)$, with $C = 4.9 \times 10^{-4}$ eV/K^2 and $T_0 = 655$ K [30]. Thus, its effect becomes negligible ($<10^{-3}$ eV) below 30 K. The last term in Eq. (C1) is the band gap narrowing due to the impurity doping. This effect has been measured for heavily B doped Si substrates at low temperatures (<20 K) using optical techniques [27,28], which do not suffer from the TIBB. The measurement reveals that the gap narrowing $\Delta E_g(n)$ of Si substrates whose B concentrations are as large as in our sample [$n = (1\text{–}2) \times 10^{19}$ cm^{-3}] is 0.06–0.09 eV. Thus, $E_g^{\rm (optical)} = 1.08\text{–}1.11$ eV from Eq. (C1).

On the other hand, Fig. 7 illustrates the TIBB effect on the band gap determination via the STS technique. Here E_F is located near the valence band (VB) edge, as is the case for our sample. When the sample bias is close to E_F, the TIBB is negligible, so that the Si substrate maintains the ground-state band profile [see Fig. 7(a)]. If the sample bias is raised to the conduction band (CB) edge [see Fig. 7(b)], however, the TIBB becomes appreciable enough to modify the band profile of the local region under the STM tip where the electron tunneling takes place predominantly. This TIBB effect would make the band gap slightly deviate or exaggerated from the genuine value.

Figure 8(a) shows the same dI/dV spectra as those in Fig. 2(d) of the main text, and the corresponding current I spectra are displayed in Fig. 8(b). It is noteworthy that the spectra in Figs. 8(a) and 8(b) are measured with a bias

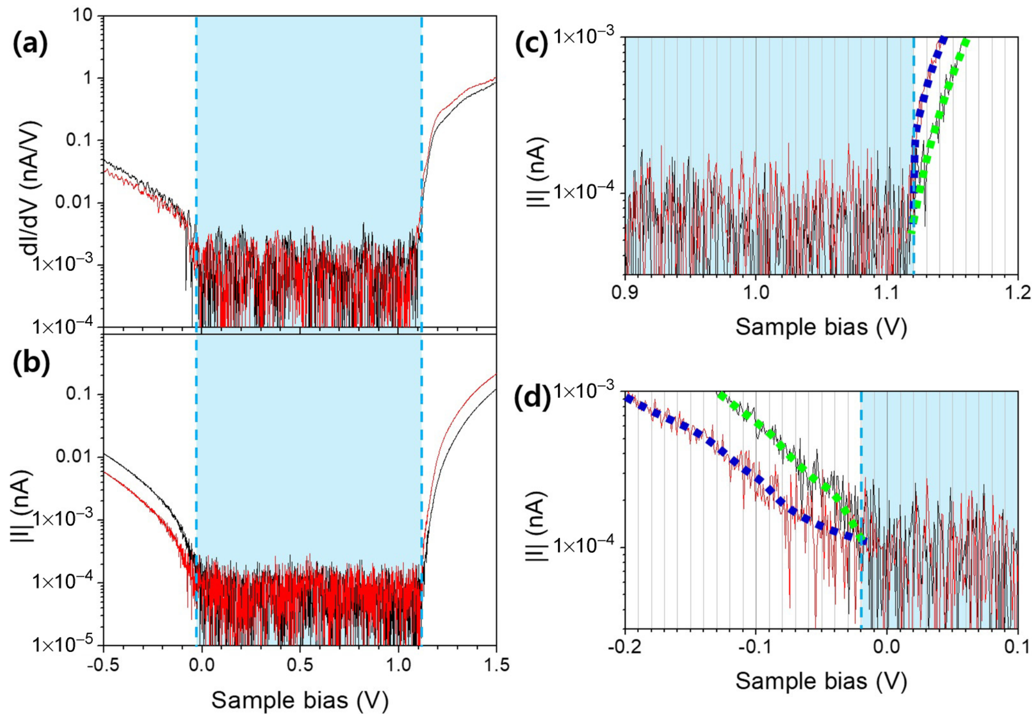

FIG. 8. (a) dI/dV spectra, which are identical to those in Fig. 2(d) of the main text. (b) Current I spectra obtained simultaneously with the dI/dV ones in (a). The vertical lines indicate the CB and VB edges. (c) and (d) Blown-up images of (b) near the CB and VB edges, respectively. The dotted lines are the best fits to the data. All the spectra in (a)–(d) are measured with a bias resolution of 1 mV.

resolution of 1 mV. Also blown-up images of Fig. 8(b) near the band edges are rendered in Figs. 8(c) and 8(d), where the dotted lines are the best fits to the original data. A careful inspection of these spectra reveals that the band gap of our sample, when determined by the STS technique, is $E_g^{(STS)} = 1.14\ \text{eV} \pm \Delta E_g^{(STS)}$ with $\Delta E_g^{(STS)} < 0.02$ eV.

[1] E. G. Seebauer and K. W. Noh, Mater. Sci. Eng. R **70**, 151 (2010).

[2] H. Y. H. Chan, K. Dev, and E. G. Seebauer, Phys. Rev. B **67**, 035311 (2003).

[3] I.-W. Lyo and P. Avouris, Science **253**, 173 (1991).

[4] H. Uchida, D. Huang, F. Grey, and M. Aono, Phys. Rev. Lett. **70**, 2040 (1993).

[5] C. Z. Wang, B. C. Pan, J. B. Xiang, and K. M. Ho, Surf. Sci. **436**, L697 (1999).

[6] K. Dev and E. G. Seebauer, Surf. Sci. **538**, L495 (2003).

[7] G. D. Watkins and J. R. Troxell, Phys. Rev. Lett. **44**, 593 (1980).

[8] G. A. Baraff, E. O. Kane, and M. Schlüter, Phys. Rev. B **21**, 3563 (1980).

[9] L. Chen, B. C. Pan, H. Xiang, B. Wang, J. Yang, J. G. Hou, and Q. Zhu, Phys. Rev. B **75**, 085329 (2007).

[10] I.-W. Lyo, E. Kaxiras, and Ph. Avouris, Phys. Rev. Lett. **63**, 1261 (1989).

[11] R. L. Headrick, I. K. Robinson, E. Vlieg, and L. C. Feldman, Phys. Rev. Lett. **63**, 1253 (1989).

[12] D. Eom, C.-Y. Moon, and J.-Y. Koo, Nano Lett. **15**, 398 (2015).

[13] J. W. Corbett and G. D. Watkins, Phys. Rev. **138**, A555 (1965).

[14] G. D. Watkins and J. W. Corbett, Phys. Rev. **138**, A543 (1965).

[15] A. Antonelli, E. Kaxiras, and D. J. Chadi, Phys. Rev. Lett. **81**, 2088 (1998).

[16] D. Eom, E. Seo, and J.-Y. Koo, Phys. Rev. B **94**, 195308 (2016).

[17] N. A. Pradhan, N. Liu, C. Silien, and W. Ho, Phys. Rev. Lett. **94**, 076801 (2005).

[18] K. Teichmann, M. Wenderoth, S. Loth, R. G. Ulbrich, J. K. Garleff, A. P. Wijnheijmer, and P. M. Koenraad, Phys. Rev. Lett. **101**, 076103 (2008).

[19] W is the intersite Coulomb energy of two electrons when they occupy two different DB orbitals. Generally, it is much smaller than the on-site Coulomb energy for which two electrons occupy a single DB orbital.

[20] Since the underlying B atom at the S_5 site is negatively charged, the net charge state of the AV would be +1 in the ground state.

[21] G. A. Baraff and M. Schlüter, Phys. Rev. Lett. **41**, 892 (1978).

[22] M. Lannoo, G. A. Baraff, and M. Schlüter, Phys. Rev. B **24**, 955 (1981).

[23] N. Nilius, T. M. Wallis, M. Persson, and W. Ho, Phys. Rev. Lett. **90**, 196103 (2003).

[24] J. C. Slater and G. F. Koster, Phys. Rev. **94**, 1498 (1954).

[25] L. F. Mattheiss and J. R. Patel, Phys. Rev. B **23**, 5384 (1981).

[26] M. Lax and E. Burstein, Phys. Rev. **100**, 592 (1955).

[27] J. Wagner, Phys. Rev. B **29**, 2002 (1984).

[28] J. Wagner, Phys. Rev. B **32**, 1323 (1985).

[29] Y. P. Varshni, Physica **34**, 149 (1967).

[30] S. M. Sze and K. K. Ng, *Physics of Semiconductor Devices*, 3rd ed. (Wiley, Hoboken, NJ, 2007).